Applied Surface Science 475 (2019) 587–597

Contents lists available at ScienceDirect

Applied Surface Science

journal homepage: www.elsevier.com/locate/apsusc

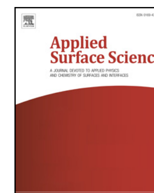

Full Length Article

A comprehensive study on electrochemical polishing of tungsten

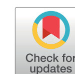

Fang Wang[a,b], Xinquan Zhang[c], Hui Deng[a,*]

[a] Department of Mechanical and Energy Engineering, Southern University of Science and Technology, No. 1088, Xueyuan Road, Shenzhen, Guangdong 518055, China
[b] Department of Mechanical Engineering, University of Hong Kong, Hong Kong 999077, China
[c] Singapore Institute of Manufacturing Technology, 71 Nanyang Drive, 638075, Singapore

ARTICLE INFO

Keywords:
Tungsten alloy
Electrochemical polishing
Crystallographic etching
Brightening
Pitting

ABSTRACT

Tungsten is a promising material for the mold of glass components owing to its excellent mechanical and chemical properties. Electrochemical polishing (ECP) has been proposed for the damage-free and highly efficient surface finishing of tungsten. In the paper, a comprehensive study of the anodic behaviors of tungsten during ECP under different applied potentials has been carried out. A mirror surface with a Sa roughness of 3.73 nm has been obtained by ECP for 10 mins demonstrating its effectiveness. The changes of surface morphology, roughness and electric current under different potentials have been experimentally investigated and analyzed. On the basis of the changes of surface morphology and current density, ECP of tungsten was divided into 3 stages including the etching stage in which rough etching marks were formed by crystallographic etching, the brightening stage in which ultra-smooth surfaces with clear boundaries were obtained and the pitting stage in which crystallographic pitting occurred. The probable material removal mechanisms of these 3 ECP stages were proposed and experimentally validated. The presented findings are of great value for understanding and process development of ECP of tungsten.

1. Introduction

Tungsten alloy with excellent physical and chemical properties of high strength, low coefficient thermal expansion and strong chemical inertness has been widely used in the fields of aerospace, electronics and chemical engineering and so forth. Especially, tungsten is the most appropriate material for the fabrication of welding electrodes, filaments, cathode for electronic tubes and valve, high temperature resistance furnace heating elements owning to its highest melting point of all metals [1].

Recently, the application of tungsten has been expanded to the fabrication of glass molds, especially for molding of glass lens with aspheric profiles which are difficult to machine with conventional machining processes like cutting, grinding and polishing [2]. Typically, the general material for glass mold is sintered tungsten carbide (WC) [3,4] or chemical vapor deposited silicon carbide (CVD-SiC) [5,6] owing to their high hardness and low thermal expansion coefficient. However, ultra-precision microstructures with sharp edges and mirror surface quality are difficult to obtain by traditional grinding and polishing [7] and the diamond cutting are also not applicable because of rapid tool wear [8]. Although the high hardness allowed the mold to be used many more times before deforming during processing, it also makes the manufacturing more difficult and time consuming. Another disadvantage of WC and SiC is that specific coatings are needed to prevent the adhesion of glass on the mold [9,10]. Ni-P [11] alloy is another widely used material to manufacture glass mold, but the thin plated layer cannot tolerate relatively high temperature which limits its application for molding of glasses with high transition points. Therefore, new molding materials with good machinability and excellent molding performance are strongly required.

Tungsten alloy possesses an ultrahigh melting point, excellent oxidation resistance under high temperature and low coefficient of thermal expansion making it a promising material to fabricate ultra-precision mold for glass components. Even though its hardness is lower than that of conventional mold materials like WC and SiC, it is hard enough for molding of most types of glasses and its relatively lower hardness makes the machining not so difficult. Meanwhile, owing to its excellent thermal chemical resistance, specific coatings are not needed to protect the mold surface. Therefore, using tungsten as the mold material for molding of glass components is very promising.

Working as a mold, an ultra-smooth surface with less subsurface damage and good form accuracy is indispensable. Grinding or mechanical polishing (MP) using hard abrasives are widely used as the rough finishing process for glass molds [12]. To remove the SSD introduced by grinding or MP and improve the surface roughness, a fine finishing process is indispensable [13]. Chemical mechanical polishing

* Corresponding author.
E-mail address: dengh@sustc.edu.cn (H. Deng).

https://doi.org/10.1016/j.apsusc.2019.01.020
Received 29 September 2018; Received in revised form 29 December 2018; Accepted 2 January 2019
Available online 03 January 2019
0169-4332/ © 2019 Elsevier B.V. All rights reserved.

(CMP) has been widely used as the fine finishing process for semiconductor wafers, optical components and molds [14,15]. However, its low polishing efficiency and the large amounts of consumed slurry makes CMP a high cost finishing approach. Meanwhile, as mechanical removal is still involved in CMP, the introduction of SSD can be suppressed but can't be eliminated. To realize the highly efficient and high quality finishing of tungsten, electrochemical polishing (ECP) [16,17] which is a slurry free polishing process has been applied. In previous study, a two-step ECP process combining the current-driven mode and potential-driven mode has been proposed to obtain a smooth tungsten surface with high efficiency [18]. A smooth surface with Sa roughness of 17.6 nm has been obtained with ECP of 23 mins demonstrating that ECP is a quite promising approach for the finishing of tungsten.

For the process development of the ECP process of tungsten, a good understanding of the polishing process is necessary. When ECP has been applied to polish many other metals such as nickel [19], iron [20], titanium [21], stainless steel [22], copper [23] and aluminum [24] and so forth, except the anticipated polishing effect, other unexpected dissolved states were also discovered [25]. In order to understand the ECP process and clarify the polishing mechanism of tungsten, a systematic study of the anodic polarization process of tungsten alloy is studied and the results are presented as well as the proposed etching models.

2. Experimental

The tungsten substrates used in this study were cut from a tungsten alloy sheet (> 99.999%) with a rectangle square of 500 mm^2 (20 mm width and 25 mm length). Fig. 1 shows the experimental setup used in this study. A glass beaker was used as the container of electrolyte to perform the etching process. The tungsten substrate was connected with the anode of the direct power source and a platinum sheet (20 mm × 20 mm) worked as the cathode. A manual vertical lifting platform was used to control the immersing depth of the substrate to insure all of the downward end face was completely immersed in electrolyte. The substrate was inclined of 30 degrees to prevent the adhering of bubbles generated by water dissolution during ECP. The distance between the substrate center and the counter electrode was 200 mm. Keysight E3649A dual output DC power supply provided electric potential to conduct electrochemical etching and the anodic polarization system was connected to a computer recording the potential and current data. After anodic etching, samples were rinsed in deionized water and dried by N_2 blowing.

ECP of the tungsten alloy is an electrochemical etching process and it is based on the simultaneous anodic oxidation and dissolution. The oxidation product of tungsten WO_3 can be dissolved in alkaline solutions. NaOH solution was used in study to perform electrochemical etching of tungsten. The electrochemical reactions occurring on the

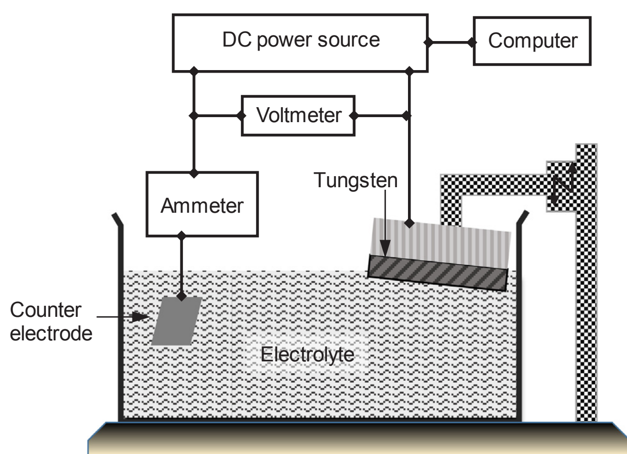

Fig. 1. Schematic of ECP setup.

platinum sheet (cathode) and tungsten (anode) can be expressed as follows:

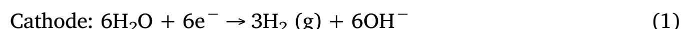

$$\text{Cathode: } 6H_2O + 6e^- \rightarrow 3H_2\ (g) + 6OH^- \quad (1)$$

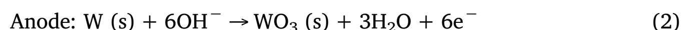

$$\text{Anode: } W\ (s) + 6OH^- \rightarrow WO_3\ (s) + 3H_2O + 6e^- \quad (2)$$

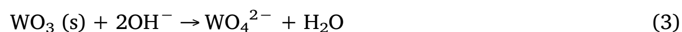

$$WO_3\ (s) + 2OH^- \rightarrow WO_4^{2-} + H_2O \quad (3)$$

Anodizing as Eq. (2) occurred on the surface of tungsten and tungsten was oxidized to WO_3. The generated WO_3 reacted with the electrolyte (NaOH) and got dissolved as Eq. (3). The hydrogen ion accumulated near the cathode and was reduced to hydrogen as Eq. (1).

Before and after ECP, the surface morphology was measured by a scanning electron microscopy (SEM, Hitachi S-4800) and the surface roughness was measured by scanning white light interferometer (Taylor Hobson M112-4449-02 CCI HD).

3. Results and discussion

3.1. The effectiveness of ECP

To examine the effectiveness of ECP for flattening of tungsten, ECP with an applied potential of 60 V in 5 wt% NaOH was carried out on a diamond ground tungsten substrate. Fig. 2 shows the morphology changes during ECP with different durations. In order to observe the same area after each polishing experiment, a rhombus indent mark as shown in Fig. 2(a) was formed on the original surface. It can be found that after polished for 10mins, the surface started to be flattened and some shallow grinding marks were already disappeared as shown in Fig. 2(b). Then, with the increase of the polishing duration, the surface was gradually smoothened. Until the polishing process continued for 30mins, the indent mark disappeared and the whole surface was thoroughly flattened as shown in Fig. 2(d). Fig. 2(e) and (f) show the photographs of the substrate before and after ECP. It has been demonstrated that a mirror tungsten surface can be obtained using ECP. These results shown in Fig. 2 revealed that ECP was effective in the flattening of tungsten.

3.2. The potential influence during ECP

Although the results shown in Fig. 2 have proved that tungsten could be polished by ECP, the polishing mechanisms and the key parameters affecting the polishing process were still unknown. As ECP is an electrochemical etching process driven by the anodic potential, the anodic potential charged on the tungsten substrate has been considered an important parameter, thus, the potential influence was firstly investigated. A series of polishing experiments under different anodizing potentials were carried out. The applied potential was increased from 1 V to 60 V and the etching duration was 10 mins for each ECP experiment. During ECP with different applied potential, the current and potential data were recorded. After ECP, the surface morphology was observed using SEM and the surface roughness was evaluated using scanning white light interferometer (SWLI).

Fig. 3 illustrates the typical surface morphology of tungsten after ECP with different applied potentials. As shown in Fig. 3(a), the as-received surface was processed by EDM wire cut and the surface was strongly damaged. When the applied potential was 3 V, the polished surface was still very rough and polishing effectiveness has not been found as shown in Fig. 3(b). When the applied potential was 10 V, a distinctly different surface was obtained. As shown in Fig. 3(c), the polished surface was very smooth and tungsten grains with different contrast as well as the grain boundaries could be observed clearly. Then, when the applied potential was 60 V, though the tungsten grains can still be observed, the processed surface was fully covered by nano-sized pits as shown in Fig. 3(d).

According to the results shown in Fig. 3, it has been revealed that

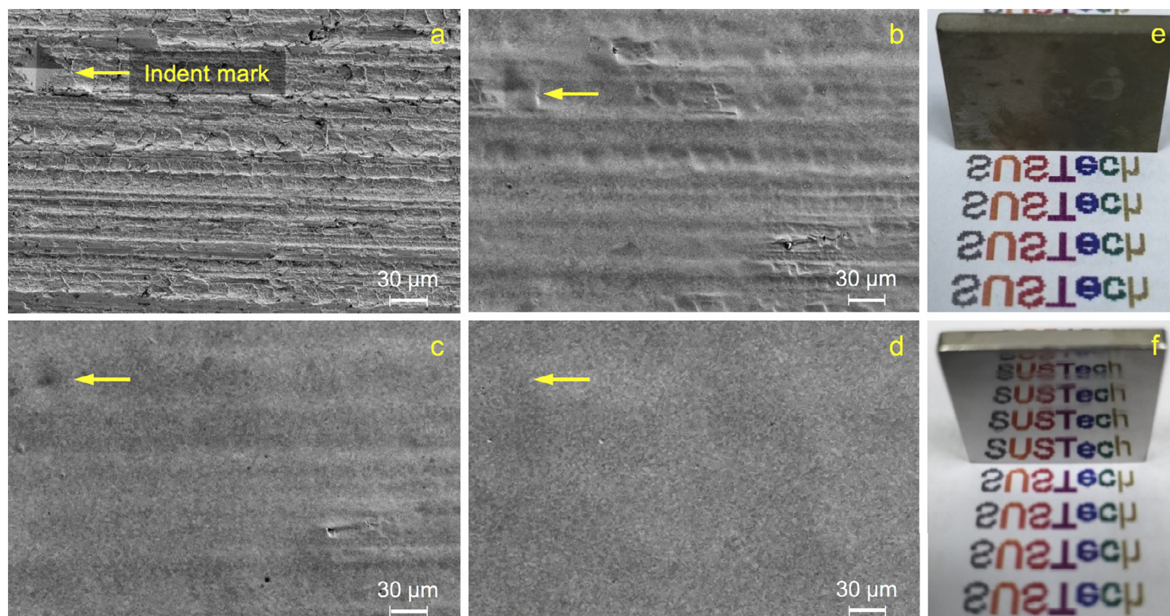

Fig. 2. a–d: Surface morphology change during ECP observed by SEM (a: as-ground surface; b: ECP for 10 mins; c: ECP for 20 mins; d: ECP for 30 mins). e: Photo of original substrate. f: Photo of ECP processed substrate.

the applied anodizing potential is a key parameter for the ECP process. Under a relatively low applied potential like 3 V, the processed tungsten surface was etched but not polished. Correspondently, when the applied potential was high enough like 60 V, the surface became smooth, however dense pits which deteriorated the surface integrity appeared. It was considered that the applied potential must be located in an intermediate potential range to form a smooth and pit-free tungsten surface.

The surface roughness of tungsten processed by ECP was measured by SWLI to quantitatively evaluate the polishing effect under different potentials. Fig. 4 illustrates the SWLI images of the surface polished under the potential of 1 V, 3 V, 10 V and 60 V. When the applied potential was 1 V or 3 V, the processed surface was very rough and many micrometer order protrusions were formed on the surface which coincided with SEM images shown in Fig. 3. When the potential was 10 V, the Sa roughness has been greatly reduced to 11.97 nm. Some protrusions can also be observed on the processed surface due to the insufficient etching. When the applied potential was increased to 60 V, an ultra-smooth surface with a Sa roughness of 3.73 nm was obtained. The cross sectional profiles reveals that high frequency roughness was formed when the applied potential was 1 V or 3 V. However, when ECP was conducted at an applied potential of 10 V or 60 V, high frequency roughness was completely removed and the profiles became very

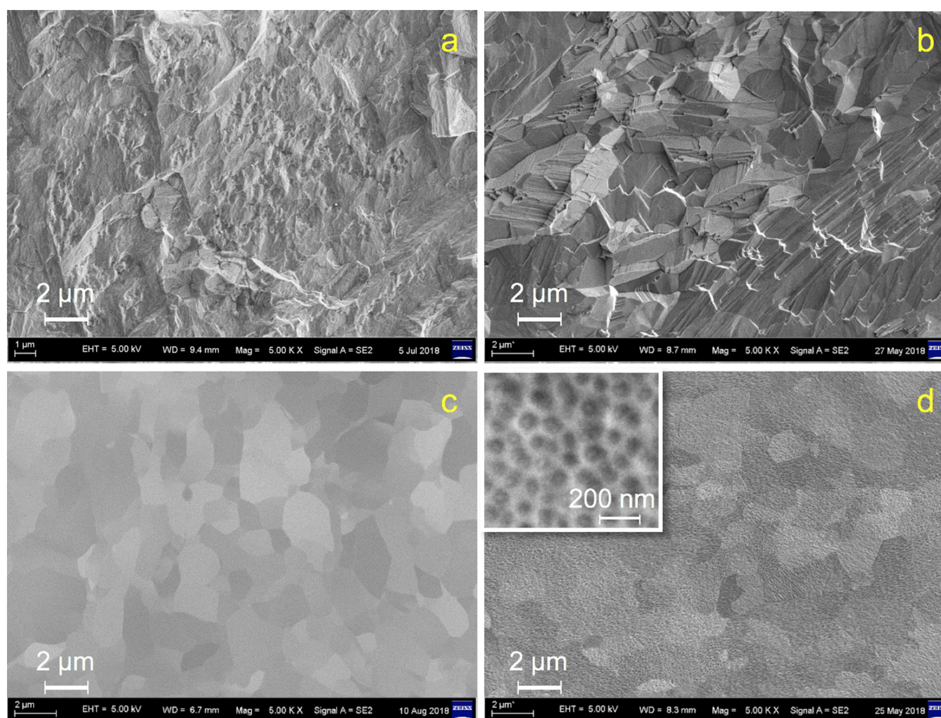

Fig. 3. Surface morphologies of tungsten observed by SEM. a: original surface; b: ECP with potential of 3 V; c: ECP with potential of 10 V; d: ECP with potential of 60 V, the inset shows a close up view of the nano-sized pits.

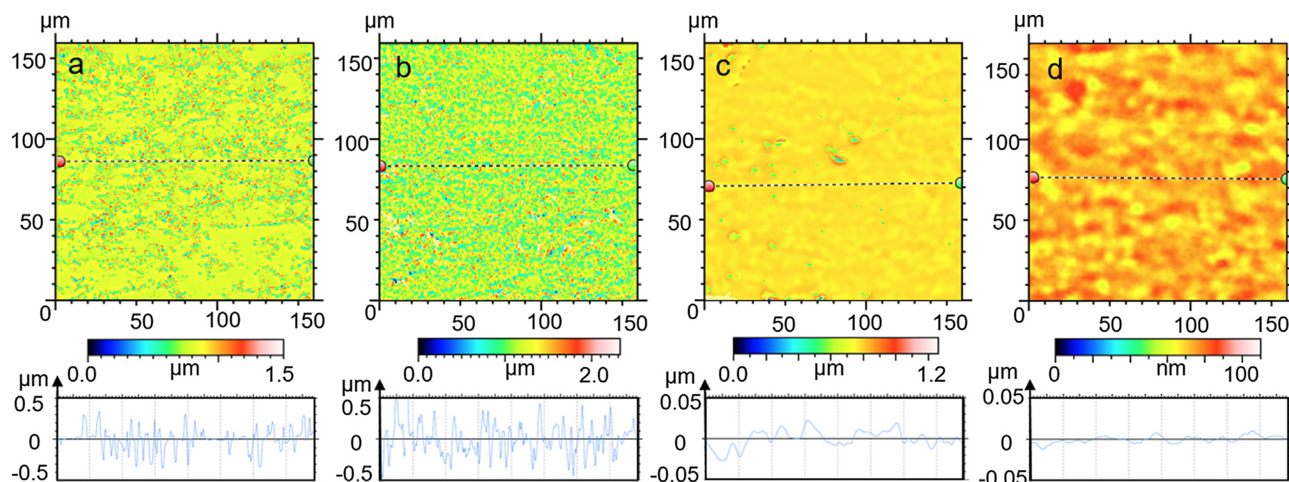

Fig. 4. SWLI images of tungsten surface processed by ECP with different applied potentials. (a) 1 V (Sa: 78.05 nm); (b) 3 V (Sa: 168.46 nm); (c) 10 V (Sa: 11.97 nm); (d) 60 V (Sa: 3.73 nm).

smooth. The small etch pits shown in Fig. 3 couldn't be observed using SWLI owing to its limitation of lateral resolution.

The dependency of surface roughness on the applied potential during the whole potential range from 1 V to 60 V has been shown in Fig. 5. It was found that with the increase of the potential, the surface Sa roughness firstly increased and the surface was the most rough (Sa: 177.32 nm) when the potential was 4 V. Then, with the further increase of the applied potential, the Sa roughness decreased drastically from 177.32 nm to 24.85 nm. When the potential was higher than 5 V, the Sa roughness only slightly decreased with the increase of the applied potential. With the potential continuous increasing up to 60 V, the Sa roughness was stable around 4 nm, indicating that an ultra-smooth surface has been obtained. Though it was found that many pits were generated under high applied potential as shown in Fig. 3(d), the formation of these dense pits did not deteriorate the surface roughness.

As reported in previous research, while the applied potential greatly affected the surface morphology, the current during ECP was the deterministic factor of the electrochemical etching rate [18]. Fig. 6 illustrates the current and current efficiency variation of ECP with different applied potentials. In this study, the polishing duration for each experiment was 10 mins. It was found that the current fluctuated drastically during the early ECP stage and in the last 5 mins the current tended to be stable. During ECP, the current was a subordinated parameter which was mainly driven by the potential and the solid-liquid interface conditions. However, as current was originated from the transition of charged species, the change of current can represent the

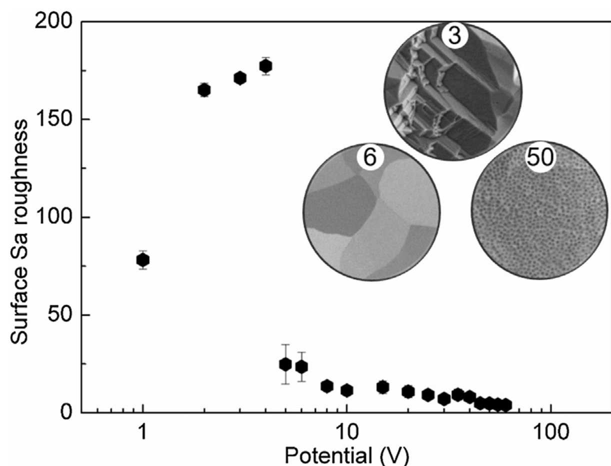

Fig. 5. Dependency of surface Sa roughness under the applied potential.

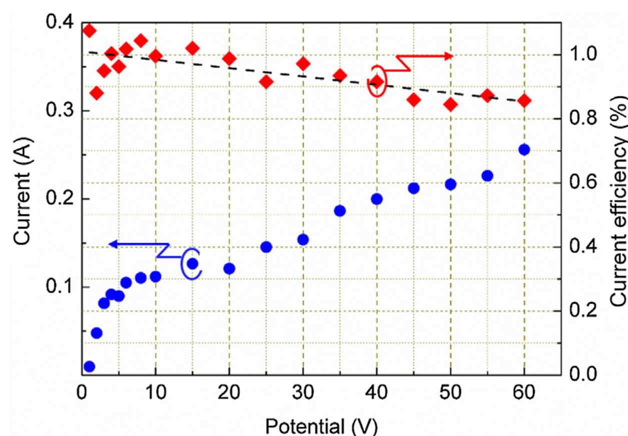

Fig. 6. Dependency of current and current efficiency under the applied potential of ECP.

condition change of the solid-liquid interface. When the current became stable, it meant that the etching of tungsten, dissolution of the etching products (WO_4^{2-}) and diffusion of WO_4^{2-} and OH^- occurring on the solid-liquid interface got balanced. Thus, the average current of the last 5 mins of ECP was calculated and its dependency under the applied potential was plotted as shown in Fig. 6 marked by blue dots. During ECP, gas bubbling around the electrode was observed. It means that water dissociation also occurred besides the etching of tungsten. Thus, current efficiency must the investigated for monitoring of the ECP process. As the current-time curves was recorded during ECP, the quantities of electric charge under different potentials can be calculated ($Q = I \times t$). As the etching mass were also measured using a precision balance, the current efficiency can be calculated by the following Eq. (4):

$$\eta = 100\% \times m'/m = 100\% \times m'/(I \times t \times k) \quad (4)$$

In Eq. (4), η represents the current efficiency, m' represents the measuring etching masses, m represents the theoretical etching masses and k represents electrochemical equivalent of tungsten. The current efficiencies under different potentials were calculated and the results were shown in Fig. 6 marked by red rhombus.

It can be found from Fig. 6 that when the potential was lower than 5 V, the current increased steeply with the increase of potential. Then, among the potential range between 5 V and 20 V, the current kept stable around 0.12A. After the potential exceeded 20 V, the second steep increasing of current occurred and in the potential range between

25 V and 60 V, the current kept increasing constantly. Current efficiency fluctuated and errors existed as the etching masses were too small under low applied potentials especially when the potential was lower than 10 V. However, an overall decreasing trend has been demonstrated with the increase of the potential. Under a higher applied potential, the dissociation of water was more aggressive and the current efficiency was slowing down.

On the basis of the etched surface morphology shown in Figs. 3 and 4 and the current variation shown in Fig. 6, ECP of tungsten with different potential can be divided into several stages. When the potential was lower than 5 V, the processed surface was roughly etched and there was no polishing effect and it was considered as the etching stage. Then, in the current-holding stage when the applied potential was in the range from 5 V to 20 V, a smooth tungsten surface with clear grain boundaries was obtained. This stage was considered as the brightening stage in which the surface roughness could be drastically improved. Finally, when the applied potential was further increased to be higher than 25 V, etch pits with a nanometer diameter were generated and the amount of the pits increased with the increase of the potential from 25 V to 60 V. This stage was defined as the pitting stage in which the ECP-processed surface was still smooth but etch pits were gradually formed. When ECP was applied to polish other metal materials, similar stage dividing has been widely reported [26]. In following chapters, the anodic behaviors and assumed etching models of the etching, brightening and pitting stages of ECP of tungsten were presented respectively.

3.3. Etching stage of ECP

The stage, during which the current increased with the increase of the applied potential and the surface was etched but not polished was defined as the etching stage. In order to investigate how the surface was etched and found out how the etching patterns evolved with the increasing of the potential in this stage, a smooth surface obtained by ECP for 10 mins with a potential of 20 V was used as the original surface. According to Fig. 6, the potential range of the etching stage was from 0 to 5 V. Therefore, ECP with applied potential of 1 V, 2 V and 3 V were conducted for 10 min and the results were shown in Fig. 7.

It can be found that under the potential of 1 V, the surface was etched preliminarily as shown in Fig. 7(a). As the original surface was polished under the potential of 20 V leaving a rather smooth initial surface and the etching duration (10mins) was not long enough to completely etch the original smooth surface, the ECP processed surface with 1 V applied potential was not as rough as these processed by ECP with potential of 2 V or 3 V and some non-etched smooth areas can still be observed as shown in Fig. 7(a). This result also coincides with the roughness measurement results shown in Fig. 5. However, rough etching marks already can be clearly observed. By contrast, when the potential was 2 V and 3 V, the surfaces were etched deeply and the smooth areas disappeared and the surfaces were fully covered by etching marks. As shown in Fig. 7, many step-like etching marks were formed on the ECP-processed surface. Crystallographic etching can be used to explain the generation of the step-like etching marks [27–29]. Electrochemical etching can be considered as a process of atomic removal. Normally, the atoms located at energetically favored kink sits on monatomic steps situated on close packed crystal planes were more easily removed. The preferential etching along particular orientations resulted in the generation of step-like etching marks. In other words, in the etching stage, etching started from the grain boundaries where there were more dangling bonds.

To further clarify the material removal mechanism occurring in the etching stage of ECP, ECP with a potential of 2 V and a short duration of 20 s were carried out on a smooth surface polished by ECP with a potential of 20 V and the results were demonstrated in Fig. 8. There were two findings from Fig. 8. First, it has been revealed that the grain boundaries were preferentially removed. This was because of the concentrated dangling bonds along the boundaries. Second, it was also found that the top faces of tungsten grains were not uniformly etched. This was because of the different orientations of these grains [30–32]. These two findings proved that crystallographic etching was the main material removal mechanism during the etching stage of ECP.

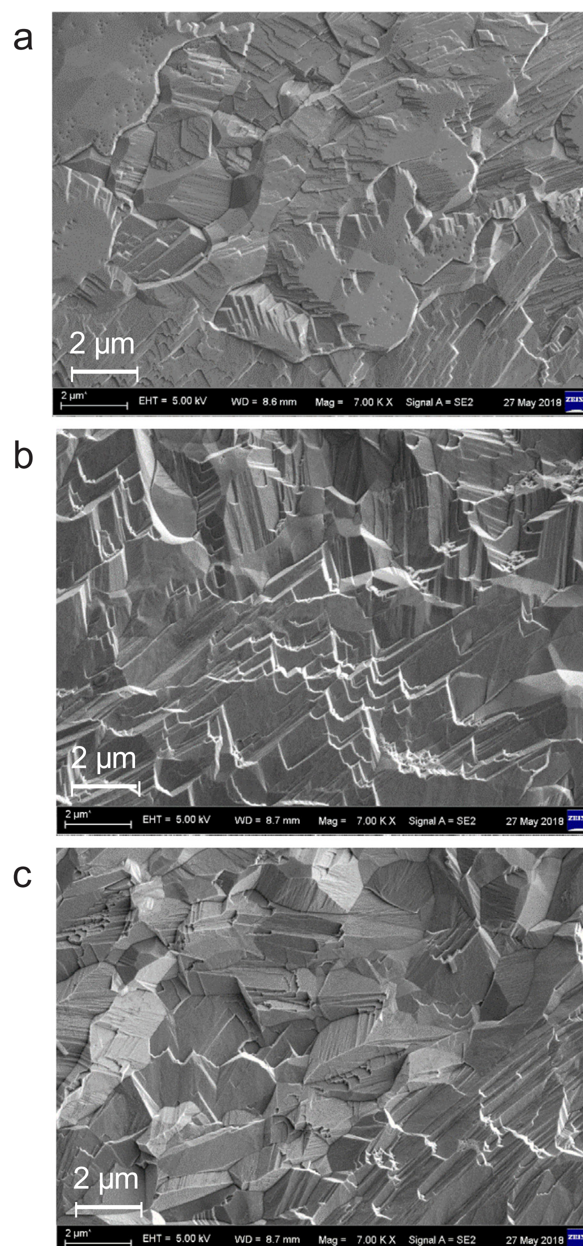

Fig. 7. SEM images of ECP-processed tungsten surfaces with potential of 1 V (a), 2 V (b) and 3 V (c).

When the potential was above 4 V but lower than 5 V, as shown in Fig. 6, the electrochemical etching occurring in ECP was located in the transition region between etching stage and brightening stage. Fig. 9 shows the surface processed by ECP with a potential of 4.2 V. The surface morphology was very different with that processed by ECP with potentials of 1 V, 2 V or 3 V as shown in Fig. 7. The surface was fully covered by etching marks. However, the step-like etching marks became shallow making the surface much more smooth than those shown in Fig. 7. It was also found that the orientations of the etching marks on different tungsten grains were different as shown in Fig. 9(b)–(e). On the basis of the different orientations of the etching marks, the grain boundaries on the surface can be clearly clarified as shown in Fig. 9(a).

When the potential was located in the transition region, the

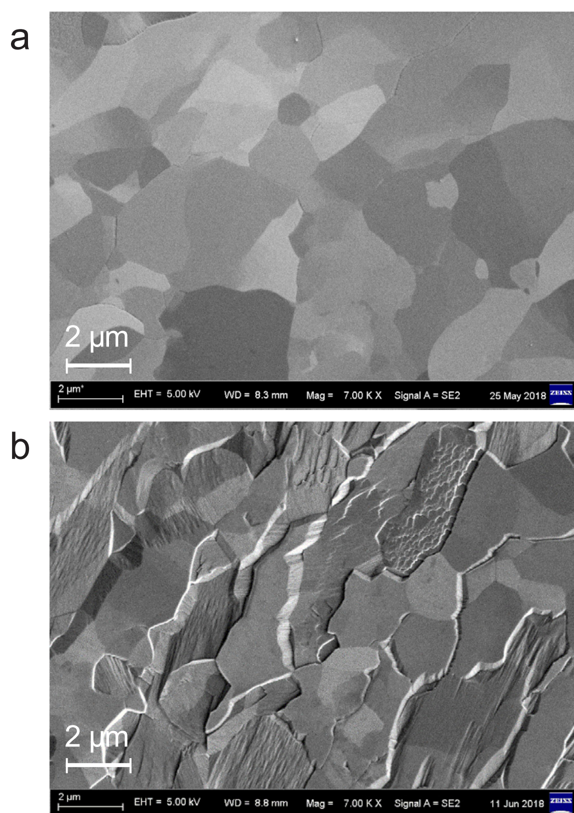

Fig. 8. SEM images of tungsten surfaces. (a) ECP for 10 mins with potential of 20 V. (b) surface (a) was further processed by ECP for 20 s with potential of 2 V.

processed surface demonstrated two distinctly different morphologies. Fig. 10(a) shows the photo of the substrate of ECP for 10 mins with a potential of 4.2 V. The central area was rough while the outer area was relatively smooth. SEM images shown in Fig. 10(b) and (c) demonstrated the difference of these two areas. Therefore, it was considered that the transition from the etching stage to the brightening stage was not an instant and homogeneous process but a gradually varied process starting from the edge area of the substrate towards the central area.

As widely reported, the flattening effectiveness of ECP was greatly dependent on the distribution of the viscous film which was generated during the electrochemical etching process. However, when ECP was under the etching stage, the processed surfaces were rough and no flattening effect was found. This was considered due to the fast dissolution of the etching products. To clarify this assumption, the changes of current during ECP were evaluated. Fig. 11 shows the current-time curves during ECP with different potentials from 1 V to 5 V. The generation of the viscous film was owing to the gathering of the etching products like WO_4^{2-} and the viscous film was nonconductive. As shown in Fig. 11, when the applied potential was 1 V, 2 V or 3 V, the current was constant during the whole etching process. It meant that the generation speed of the etching products was lower than its dissolution speed. As of the result, the nonconductive viscous film wasn't formed and no flattening effect existed. When the applied potential was 5 V, the current firstly dropped sharply and then kept stable at a little higher current level, which was a typical flattening current curve. The steep decrease of the current demonstrated the formation of the viscous film and the final constant value at a higher level indicated that the ion diffusion and metal dissolution was balanced and the thickness of the film was constant resulting in excellent polishing effect. However, in the transition potential region with the potential of 4 V, the little drop of current was detected but the stable value did not have a slight increase, which means that although the viscous film was formed, its conductivity was not improved leading to the film in barely satisfactory

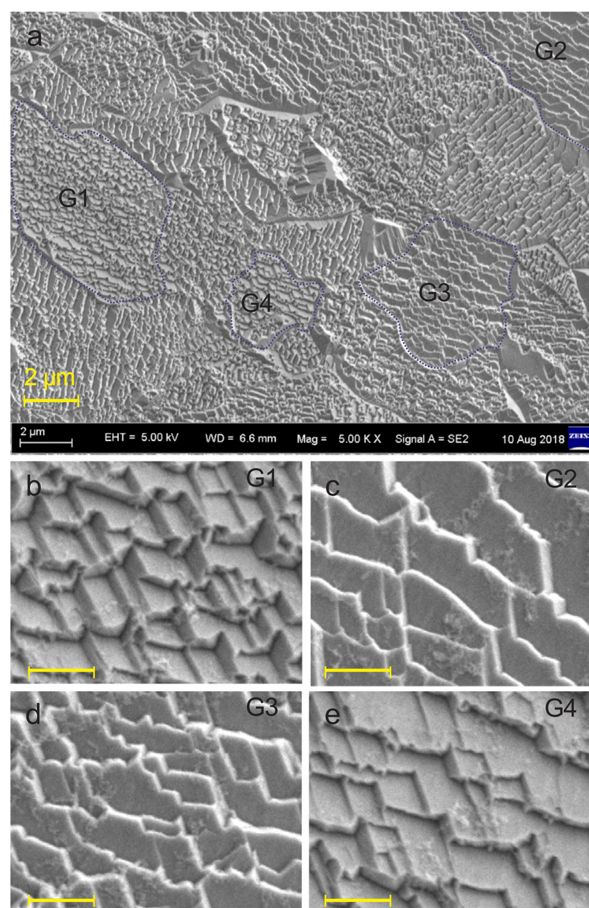

Fig. 9. SEM images of tungsten surface processed by ECP with potential of 4.2 V. (a) The overall image. (b–e) Enlarged images of the etching marks on G1, G2, G3 and G4, the scale bars were 400 nm.

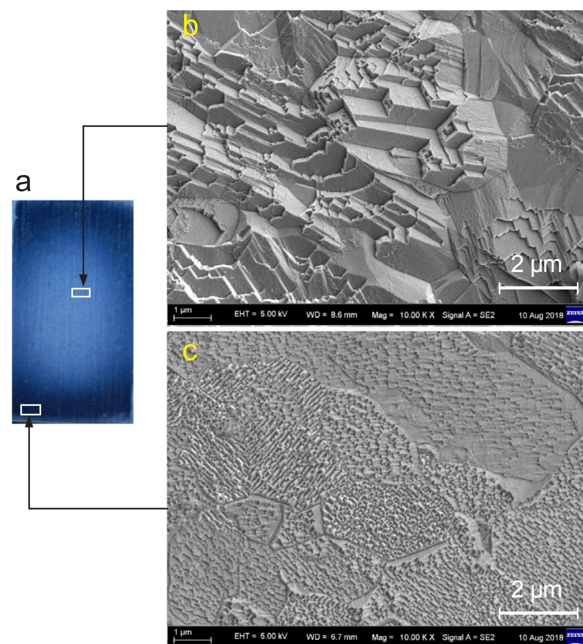

Fig. 10. Photograph and SEM images of tungsten surface processed by ECP with potential of 4.2 V. (a) The photograph of the substrate. (b) SEM image of the substrate central area. (c) SEM image of the substrate edge area.

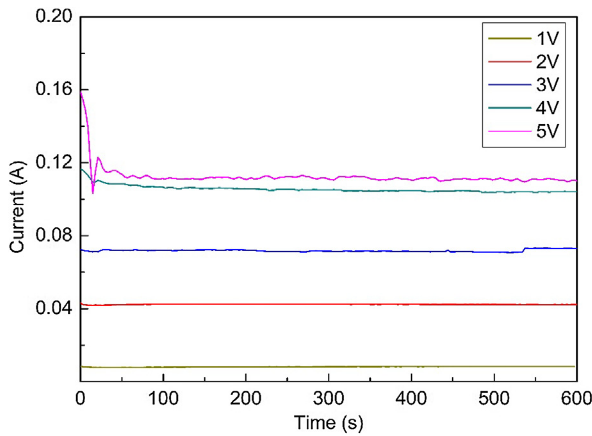

Fig. 11. Current-time curves of ECP under different potentials from 1 V to 5 V.

flattening effect. This can explain why the processed surfaces were relatively smooth when the applied potentials were located in the transition region.

Based on the above results, it was concluded that crystallographic etching was the main material removal mechanism during the etching stage of ECP when the applied potential was located in the range from 0 to 5 V. Fig. 12 shows the schematic model of the crystallographic etching process. It was well known that tungsten alloy was a kind of polycrystalline metal and the grains in the substrate had different crystalline orientations. G1, G2, G3, and G4 represented four typical grains with different crystalline orientations. Etching started from the grain boundaries where there were more dangling bonds. So the grain boundaries like G1/G2, G2/G3 and G3/G4 were preferentially etched. As the top surface orientations of these grains were different, the etching rates for G1, G2, G3 and G4 were also different resulting in the generation of step-like etching marks as shown in the SEM image in Fig. 12. As the etching products were dissolved once formed, flattening effect didn't exist in the etching stage of ECP.

When the potential increased to the transition region which was between 4 V and 5 V, a thin layer of viscous film was generated which could improve the surface roughness. In the transition potential region, surface roughening driven by the crystallographic etching and surface

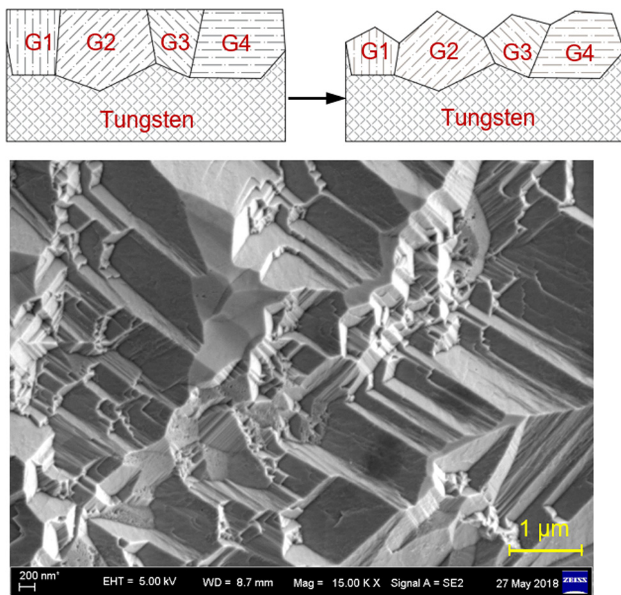

Fig. 12. Schematic of material removal mechanism of the etching stage of ECP and a typical surface morphology image observed by SEM.

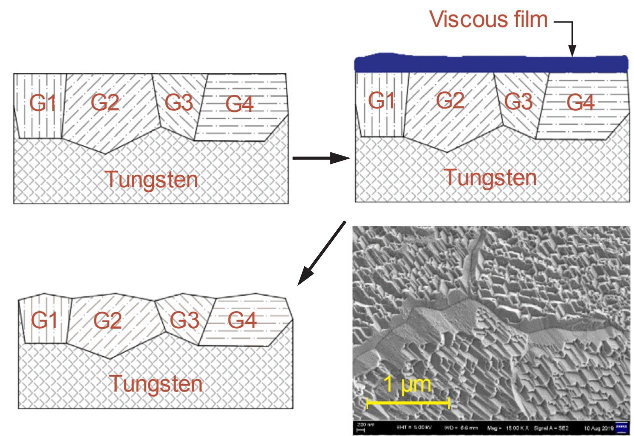

Fig. 13. Schematic of material removal mechanism of the transition region between etching stage and brightening stage and a typical surface morphology image observed by SEM.

flattening driven by the viscous film both existed. Fig. 13 shows the proposed material removal mechanism occurring in the transition potential region of ECP. The processed surface was relatively smooth but etching marks with shallow etching steps still existed.

3.4. Brightening stage of ECP

As shown in Fig. 6, when the applied potential was further increased to the range from 5 V to 24 V, a smooth surface which was free of etching marks as well as etching pits could be obtained. During this brightening stage, the surface was polished and both the current and the surface Sa roughness nearly kept constant with the increasing of the potential. Fig. 14 shows the surface morphologies which was processed by ECP for 10 mins under the potential of 6 V, 8 V, 10 V and 20 V respectively. It can be found that the surface morphologies under different potentials were almost the same. The processed surfaces were very smooth and the grain boundaries could be clearly observed.

Many hypothesis were proposed to explain the material removal mechanism of the brightening stage, among which the Jacquet theory [33], Elmore theory [34,35] and Edwards theory [36] were the most widely accepted. Jacquet's theory attributed the importance of the flatting effect to the large ohmic resistance of the viscous film. As shown in Fig. 15, when the substrate started to dissolve at an appropriate potential, a viscous film would generate on the interface of the metal and the electrolyte. As the viscous film had a large electrical resistance, the electric field distribution across the initial rough surface was non uniform. The electric field strength around the peak areas and valley areas was different. The film on the peak areas was thinner than that on the valley areas which resulted in the current density on the peaks was higher than that on the valleys. Since the dissolving rate depended on the current density, the higher current density leaded to a higher dissolving rate, thus the peak areas were preferentially etched and eventually the surface was polished.

However, according to Elmore's theory, the diffusion of metal ions owing to the varying concentration gradient over the peaks and valleys was also an important influence factor of the polishing effect. With the increase of current density caused by increased potential, the metal ion dissolving rate increased and diffused into the bulk electrolyte resulting in the increase of concentration of metal ions. As the increase of the metal ions concentration, the concentration gradient would become narrowed which limited the diffusion of metal ions. When the concentration was saturated on the metal surface, the metal dissolving rate would be determined by the diffusion rate of the metal ions displacing the current density as the key influence factor, which can be considered as a mass transport process. So after the concentration being saturated,

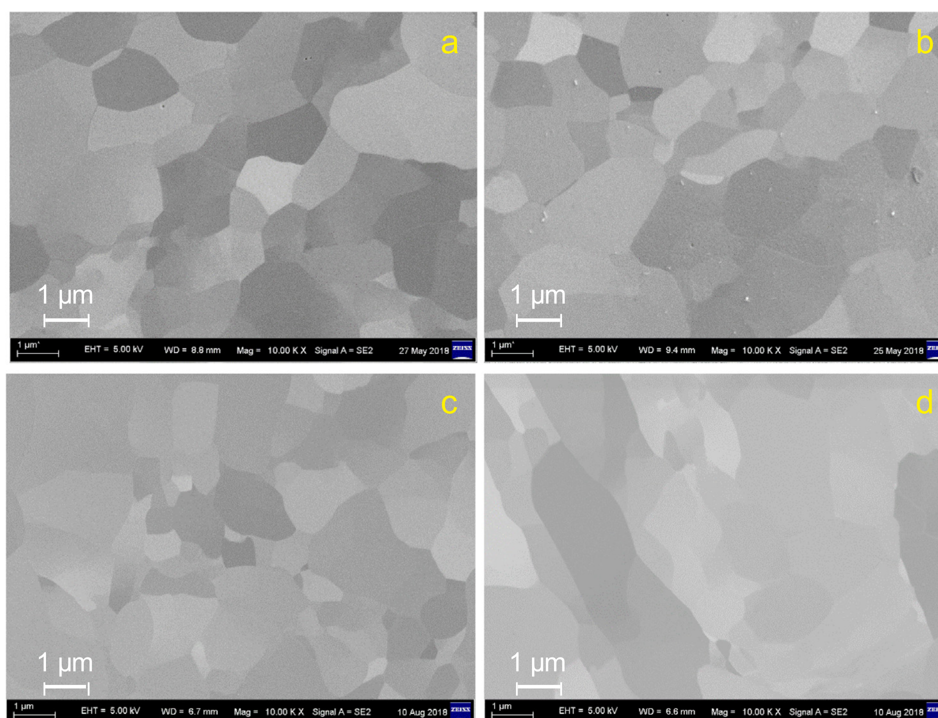

Fig. 14. SEM images of ECP-processed tungsten surfaces with potential of 6 V (a), 8 V (b), 10 V (c) and 20 V (d).

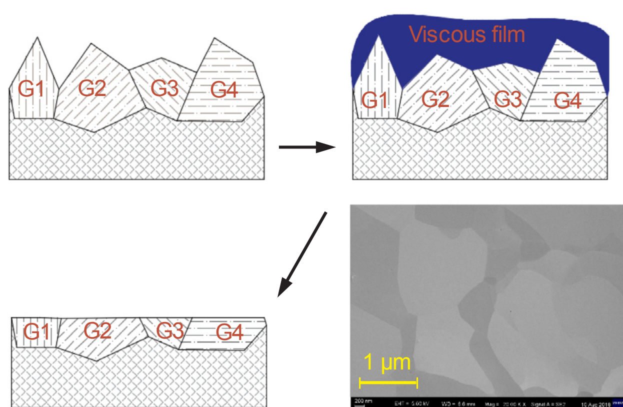

Fig. 15. Schematic of material removal mechanism of the brightening stage of ECP and the typical surface morphology image observed by SEM.

even if the potential increased, the current density would keep constant, which called a current plateau. As the thickness of the diffusion layer over peaks was smaller than that over valleys, a higher current density over the peaks versus the valleys was obtained. The higher current density over peaks leaded to the metal surface being polished. The theory proposed by Halfway and developed by Edwards was similar with Elmore's theory, what's different was that the key influence factor was given place to the depletion of anolyte layer of acceptors, anions and molecules, which had the potential to react with the metal. As continuous consumption of these anions and molecules, their concentration over the metal surface was lower than that in the bulk electrolyte resulting in the fact that the metal dissolving rate was determined by the diffusion rate of these anions and molecules. As the protrusions had more access to react with these acceptors, the protrusions were finally flattened and an even surface was obtained.

Even though different polishing mechanisms were proposed to explain the brightening stage of ECP, it was considered that ECP of tungsten was a complex process and the polishing was governed by different factors including the viscous film as well as mass transport. On the basis of these hypothesis and the fact that a colorful thin layer was observed during the polishing process it can be speculated that when the tungsten was electrolyzed, tungsten was oxidized to WO_3. Since WO_3 could be dissolved by NaOH solution, a large amount of WO^{4-} were generated. Owing to the existence of concentration gradient, the generated WO^{4-} would diffuse into the electrolyte quickly. With the diffusion of the WO^{4-}, the concentration gradient was narrowed and consequently the diffusion rate slowed down. When the diffusion rate was lower than the generating rate of WO^{4-}, lots of WO^{4-} with other ions and water would form the viscous film and by the function of the viscous film the surface was polished.

The mass transport controlling theory could be used to explain why the metal dissolving rate was dependent on the ion diffusion rate and the current density kept constant during the brightening stage. The mass transport limiting species included the metal cations or anions formed by the reduction of metal, acceptor anions consuming at the anode by the formation of metal ions and water from the bulk to the anode. In the anodic oxidation process of tungsten the anions would be OH^-, which oxidized tungsten to WO_3 and reduced the WO_3 into WO^{4-}.

ECP of tungsten was conducted using the experimental setup shown in Fig. 16 (a) to investigate the effect of the mass transport process. A sleeve made of alumina ceramic was used to support the substrate. Tungsten was located on the top of the sleeve ensuring all of the end face of the sample being immersed into the electrolyte and the inner part of the sleeve was full of electrolyte. The applied potential was 20 V and the polishing duration was 10 mins. Fig. 16(b) shows the photo of the polished surface. It can be found that the surface areas inside and outside the sleeve were different. While the outside area was shining and smooth, the inside area was very rough. Fig. 16(c) and (d) shows the surface morphologies of area c which was located inside the sleeve and area d which was located outside the sleeve respectively. For area c, many etching marks were formed which was very similar to the surface polished by ECP under the etching stage. For area d, the surface was very smooth and the grain boundaries can be clearly observed which was like a brightening polishing result.

As the tungsten surface was equipotential, the difference shown in

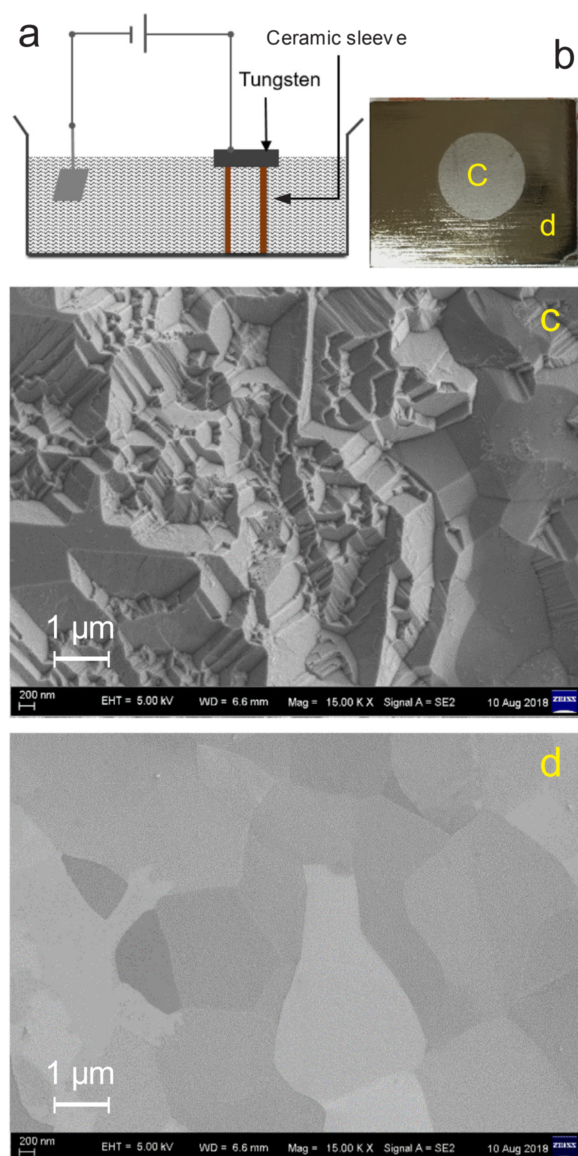

Fig. 16. ECP of tungsten with a ceramic sleeve to obstruct the mass transport. (a) Schematic of the experimental setup. (b) Photograph of the processed substrate. (c) SEM image of the area c shown in (b). (d) SEM image of area d shown in (b).

Fig. 16(c) and (d) was considered owing to the different mass transporting conditions. As by the obstructing of the sleeve, both the WO^{4-} and the OH^- could not be exchanged freely. As the limiting specie was WO^{4-}, large amounts of WO^{4-} accumulated on the surface and couldn't be diffused into the electrolyte, which resulted in the viscous film become more and more thick. Too thick of the viscous film would lead to a large electrical resistance and reduced the potential on the substrate surface, which would result in the crystallographic etching and make the surface rough. Meanwhile, with the absence of OH^-, the anodizing of tungsten would stop and the etching rate would be greatly reduced. Based on the results shown in Fig. 16, it was concluded that the formation of the viscous film as well as the mass transport process played important roles in the brightening stage of ECP.

3.5. Pitting stage of ECP

As shown in Fig. 6, in the pitting stage, pits appeared but the surface was not roughly etched and the roughness was not deteriorated. Fig. 17 shows the surface morphologies of tungsten obtained after ECP for 10 mins under the potential of 25v, 26v, 30v, 40v, 50v and 60 v. It can be found that from 25 V to 40 V pits firstly started to generate on the surface and then the surface was fully covered by the dense pits. Viewing from Fig. 17(b) and (c), it was found that the density of pits on different grains was different at the initial pitting stage. It also can be found that the pits on different grains presented different inclining directions. The above results demonstrated that the pitting stage was strongly related to the crystalline orientations of the grains in tungsten.

A lot of hypothesis were proposed to explain the formation of the pits [37–39] among which the attacking ions theory [40,41] was the most widely accepted. According to the attacking ions theory, many aggressive anions such as Cl^-, Br^- and SO^{4-} would penetrate into the viscous film under high potentials. Before the penetrating of the anions, the polishing process was controlled by the viscous film and mass transport limiting species. The metal dissolving rate was dependent on the diffusion rate of the limiting species and the crystallographic etching was restricted and tungsten grains with different orientations were etched uniformly resulting in a smooth surface. However, the penetration of anions would form some channels with good electrical conductivity. Thus, the anions penetration channels would be easily breakdown and many more anions would penetrate into the viscous film along the channels and reacted with the metal. At this point many metal atoms lost electrons and were removed to form the pits. With the increasing of the potential, more and more channels were formed leaving more and more pits on the metal surface and correspondently the current density would grow up until the surface was all covered with these pits. However, when the atoms were removed, as the anodizing along monatomic step direction was preferred, the generated pits had different growing directions, which eventually leaded to the crystallographic pitting morphology. Fig. 18 demonstrates the pitting mechanism during the pitting stage of ECP and the crystallographic pitting morphology.

4. Conclusions

In the paper, a systematic study of ECP of tungsten has been carried out. The effectiveness of ECP has been confirmed. The changes of surface morphology, roughness and electric current under different potentials have been investigated. The anodic behaviors of tungsten in different ECP stages were analyzed and the probable material removal models were proposed. To summarize, the following conclusions can be drawn from this study:

(1) As a noncontact and etching-based chemical process, ECP has been proved very effective for surface smoothening of tungsten. A mirror surface with Sa roughness of 3.7 nm was obtained by ECP with polishing duration of 10 mins.
(2) On the basis of the changes of surface morphology and current density, ECP of tungsten with different applied potentials was divided into 3 stages: etching stage, brightening stage and pitting stage.
(3) In the etching stage when the applied potential was lower than 5 V, the dissolution rate of the etching products was higher than its generation and polishing effect from the viscous film didn't exist. Crystallographic etching occurred on the surface and step-like etching marks were formed.
(4) In the brightening stage when the applied potential was located in the range from 5 V to 25 V, an ultra-smooth surface with clear grain boundaries was obtained. It has been proved that the viscous film as well as the mass transporting process played important roles to make the surface smooth.
(5) In the pitting stage when the applied potential was higher than 25 V, pits with nanometer diameters were generated though the processed surfaces were still smooth. The generation of the etch pits was considered owing to the breakdown of the viscous film by the penetration of aggressive ions.

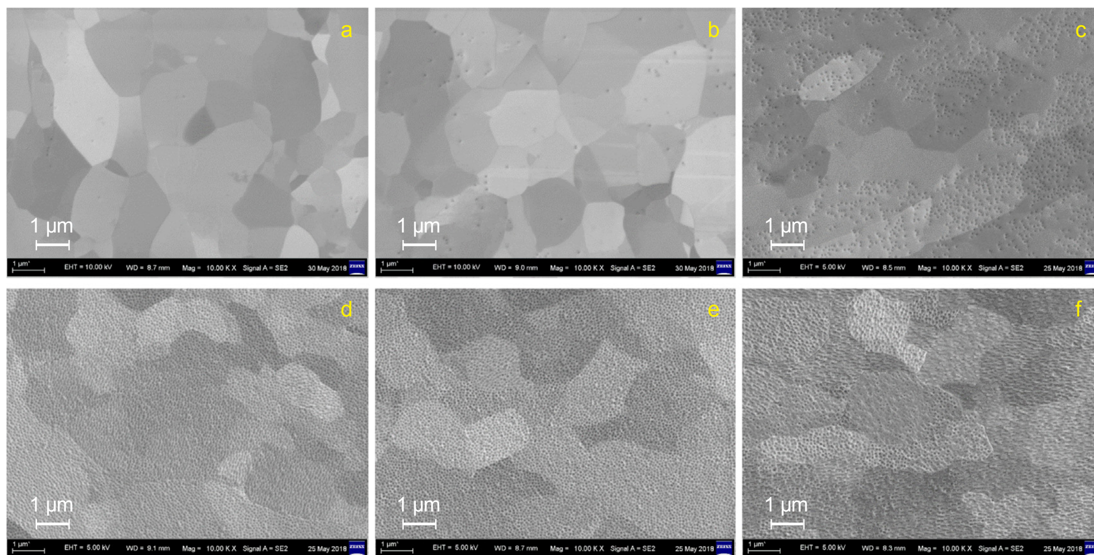

Fig. 17. SEM images of ECP-processed tungsten surfaces with potential of 25 V (a), 26 V (b), 30 V (c), 40 V (d), 50 V (e) and 60 V (f).

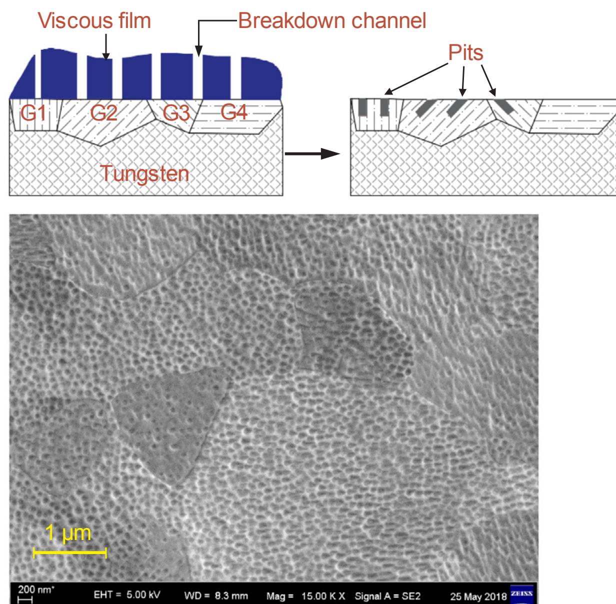

Fig. 18. Schematic of pitting mechanism of the pitting stage of ECP and a typical crystallographic pitting morphology observed by SEM.

Acknowledgements

This work was financially supported by the Start-up Funding of the Southern University of Science and Technology (33/Y01336106) and the Research Fund for International Cooperation from the Science and Technology Innovation Committee of Shenzhen Municipality (GJHZ20180411143558312). The authors would like to express our grateful thanks to the Materials Characterization and Preparation Center for the assistance in SEM observation.

References

[1] G.-M. Song, Y.-J. Wang, Y. Zhou, Thermomechanical properties of TiC particle-reinforced tungsten composites for high temperature applications, Int. J. Refract Metal Hard Mater. 21 (1–2) (2003) 1–12.
[2] N. Suzuki, M. Haritani, J. Yang, R. Hino, E. Shamoto, Elliptical vibration cutting of tungsten alloy molds for optical glass parts, Cirp Ann. – Manuf. Technol. 56 (1) (2007) 127–130.
[3] W. Choi, J. Lee, W.-B. Kim, B.-K. Min, S. Kang, S.-J. Lee, Design and fabrication of tungsten carbide mould with micro patterns imprinted by micro lithography, J. Micromech. Microeng. 14 (11) (2004) 1519–1525.
[4] H. Suzuki, S. Hamada, T. Okino, M. Kondo, Y. Yamagata, T. Higuchi, Ultraprecision finishing of micro-aspheric surface by ultrasonic two-axis vibration assisted polishing, CIRP Ann. 59 (1) (2010) 347–350.
[5] T. Itoh, S. Tanaka, J.F. Li, R. Watanabe, M. Esashi, Silicon-carbide microfabrication by silicon lost molding for glass-press molds, J. Microelectromech. Syst. 15 (4) (2006) 859–863.
[6] B. Guo, Q.L. Zhao, M.J. Jackson, Ultrasonic vibration-assisted grinding of microstructured surfaces on silicon carbide ceramic materials, Proc. Inst. Mech. Eng. Part B: J. Eng. Manuf. 226 (3) (2011) 553–559.
[7] L. Yin, H. Huang, Brittle materials in nano-abrasive fabrication of optical mirror-surfaces, Precis. Eng. 32 (4) (2008) 336–341.
[8] Y. Zhang, Z. Zhou, Y. Lv, J. Wang, L. Shao, A. Iqbal, Wear behavior of natural diamond tool in cutting tungsten-based alloy, Int. J. Adv. Manuf. Technol. 69 (1–4) (2013) 329–335.
[9] K.J. Ma, H.H. Chien, W.H. Chuan, C.L. Chao, K.C. Hwang, Design of protective coatings for glass lens molding, Key Eng. Mater. 364–366 (2007) 655–661.
[10] K.D. Fischbach, K. Georgiadis, F. Wang, O. Dambon, F. Klocke, Y. Chen, A.Y. Yi, Investigation of the effects of process parameters on the glass-to-mold sticking force during precision glass molding, Surf. Coat. Technol. 205 (2) (2010) 312–319.
[11] J. Yan, T. Oowada, T. Zhou, T. Kuriyagawa, Precision machining of microstructures on electroless-plated NiP surface for molding glass components, J. Mater. Process. Technol. 209 (10) (2009) 4802–4808.
[12] E. Brinksmeier, Y. Mutlugünes, F. Klocke, J.C. Aurich, P. Shore, H. Ohmori, Ultra-precision grinding, CIRP Ann. 59 (2) (2010) 652–671.
[13] A. Beaucamp, Y. Namba, I. Inasaki, H. Combrinck, R. Freeman, Finishing of optical moulds to λ/20 by automated corrective polishing, CIRP Ann. 60 (1) (2011) 375–378.
[14] E. Paul, Application of a CMP Model to Tungsten CMP, J. Electrochem. Soc. 148 (6) (2001) g359–g363.
[15] Y.J. Seo, N.H. Kim, W.S. Lee, Chemical mechanical polishing and electrochemical characteristics of tungsten using mixed oxidizers with hydrogen peroxide and ferric nitrate, Mater. Lett. 60 (9–10) (2006) 1192–1197.
[16] G. Yang, B. Wang, K. Tawfiq, H. Wei, S. Zhou, G. Chen, Electropolishing of surfaces: theory and applications, Surf. Eng. 33 (2) (2016) 149–166.
[17] P. Pendyala, M.S. Bobji, G. Madras, Evolution of surface roughness during electropolishing, Tribol. Lett. 55 (1) (2014) 93–101.
[18] H. Deng, R. Huang, K. Liu, X.Q. Zhang, Abrasive-free polishing of tungsten alloy using electrochemical etching, Electrochem. Commun. 82 (2017) 80–84.
[19] A. Seghiouer, J. Chevalet, A. Barhoun, F. Lantelme, Electrochemical oxidation of nickel in alkaline solutions a voltammetric study and modelling, J. Electroanal. Chem. 442 (1998) 113–123.
[20] D. Pérez Escobar, C. Miñambres, L. Duprez, K. Verbeken, M. Verhaege, Internal and surface damage of multiphase steels and pure iron after electrochemical hydrogen charging, Corros. Sci. 53 (10) (2011) 3166–3176.
[21] Z. Cai, T. Shafer, I. Watanabe, M.E. Nunn, T. Okabe, Electrochemical characterization of cast titanium alloys, Biomaterials 24 (2003) 213–218.
[22] S. Mohan, D. Kanagaraj, R. Sindhuja, S. Vijayalakshmi, N.G. Renganathan, Electropolishing of stainless steel—a review, Trans. IMF 79 (4) (2017) 140–142.
[23] J. Huo, R. Solanki, J. McAndrew, Study of anodic layers and their effects on electropolishing of bulk and electrocplated films of copper, J. Appl. Electrochem. 34 (2004) 305–314.
[24] M. Morita, T. Shibata, N. Yoshimoto, M. Ishikawa, Anodic behavior of aluminum in organic solutions with different electrolytic salts for lithium ion batteries, Electrochim. Acta 47 (2002) 2787–2793.

[25] S.Z. Chu, S. Inoue, K. Wada, S. Hishita, K. Kurashima, Fabrication of self-organized titania nanostructures on glass by bonbined anodization, J. Electrochem. Soc. 152 (3) (2005) B116–B124.
[26] D. Landolt, Fundemental aspects of electropolishing, Electrochim. Acta 32 (1) (1987) 1–11.
[27] L.D. Hulett, F.W. Young, Ledge formation on the (111) surface of copper, J. Electrochem. Soc. 113 (5) (1966) 410–415.
[28] W. Allgaier, K.E. Heusler, Steps and kinks on 211 iron surfaces and the kinetics of the iron electrode, J. Appl. Electrochem. 9 (1979) 155–160.
[29] R. Kaischew, E. Budevski, Surface processes in electrocrystallization, Contemp. Phys. 8 (5) (1967) 489–516.
[30] Henry Leidheiser, Allan T. Gwathmey, The influence of crystal face on the electrochemical properties of a single crystal of copper, Trans. Electrochem. Soc. 91 (1) (1947) 95–110.
[31] T.H. Orem, Influence of crystallographic orientation on the corrosion rate of aluminum in acids and alkalies, J. Res. Natl. Bureau Stand. 58 (1957) 157–167.
[32] A.T. Gwathmey, A.F. Benton, Some experiments showing the directional reactivities of single crystals of copper, Trans. Electrochem. Soc. 77 (1) (1940) 211–222.
[33] Jacquet, Electrolytic method for obtaining bright copper surfaces, Nature 135 (135) (1935) 1.
[34] W.C. Elmore, Electrolytic polishing, J. Appl. Phys. 10 (10) (1939) 724–727.
[35] W.C. Elmore, Electrolytic polishing. II, J. Appl. Phys. 11 (12) (1940) 797–799.
[36] J. Edwards, The mechanism of electropolishing of copper in phosphoric acid solutions, J. Electrochem. Soc. 100 (8) (1953) 223C–230C.
[37] T.R. Beck, Occurrence of salt films during initiation and growth of corrosion pits, J. Electrochem. Soc. 126 (10) (1979) 17552–17558.
[38] H.-H. Strei-Iblow, M.B. IrES, On the electrochemical conditions within small pits, Corros. Sci. 16 (5) (1976) 317–321.
[39] G.S. Frankel, Pitting corrosion of metals. A review of the critical factors, Cheminform 29 (32) (1998) 2186–2197.
[40] T.P. Hoar, The production and breakdown of the passivity of metals, Corros. Sci. 7 (6) (1967) 341–355.
[41] T.P. Hoar, D.C. Mears, G.P. Rothwell, The relationships between anodic passivity, brightening and pitting, Corros. Sci. 5 (4) (1965) 279–289.